Composition, Morphology, and Stratigraphy of Noachian Crust around the Isidis basin

J. F. Mustard,[1] B. L. Ehlmann,[1] S. L. Murchie,[2] F. Poulet,[3] N. Mangold,[4] J. W. Head,[1] J.-P. Bibring,[3] and L. H. Roach[1]

Received 29 January 2009; revised 2 July 2009; accepted 22 July 2009; published 12 December 2009.

[1] Definitive exposures of pristine, ancient crust on Mars are rare, and the finding that much of the ancient Noachian terrain on Mars exhibits evidence of phyllosilicate alteration adds further complexity. We have analyzed high-resolution data from the Mars Reconnaissance Orbiter in the well-exposed Noachian crust surrounding the Isidis basin. We focus on data from the Compact Reconnaissance Imaging Spectrometer for Mars as well as imaging data sets from High Resolution Imagine Science Experiment and Context Imager. These data show the lowermost unit of Noachian crust in this region is a complex, brecciated unit of diverse compositions. Breccia blocks consisting of unaltered mafic rocks together with rocks showing signatures of Fe/Mg-phyllosilicates are commonly observed. In regions of good exposure, layered or banded phyllosilicate-bearing breccia rocks are observed suggestive of pre-Isidis sedimentary deposits. In places, the phyllosilicate-bearing material appears as a matrix surrounding mafic blocks, and the mafic rocks show evidence of complex folded relationships possibly formed in the turbulent flow during emplacement of basin-scale ejecta. These materials likely include both pre-Isidis basement rocks as well as the brecciated products of the Isidis basin–forming event at 3.9 Ga. A banded olivine unit capped by a mafic unit covers a large topographic and geographic range from northwest of Nili Fossae to the southern edge of the Isidis basin. This olivine-mafic cap combination superimposes the phyllosilicate-bearing basement rocks and distinctly conforms to the underlying basement topography. This may be due to draping of the topography by a fluid or tectonic deformation of a previously flatter lying morphology. We interpret the draping, superposed olivine-mafic cap combination to be impact melt from the Isidis basin–forming event. While some distinct post-Isidis alteration is evident (carbonate, kaolinite, and serpentine), the persistence of olivine from the time of Isidis basin suggests that large-scale aqueous alteration processes had ceased by the time this unit was emplaced.

Citation: Mustard, J. F., B. L. Ehlmann, S. L. Murchie, F. Poulet, N. Mangold, J. W. Head, J.-P. Bibring, and L. H. Roach (2009), Composition, Morphology, and Stratigraphy of Noachian Crust around the Isidis basin, *J. Geophys. Res.*, *114*, E00D12, doi:10.1029/2009JE003349.

1. Introduction

[2] Defining the nature of the early crust on Mars remains a challenging problem. It remains uncertain whether a magma ocean existed on Mars and contributed to the formation of the crust [*Taylor et al.*, 2006] and what role volcanism played. Models of planetary evolution and crustal formation suggest that primary crust may have originally formed during cooling of a magma ocean and subsequent extensive volcanism would have formed a secondary crust [*Taylor et al.*, 2008]. While it is widely accepted that this early crust would have been broadly basaltic in composition, this originally crystalline igneous landscape has been significantly modified and reworked by impact, gradation, and tectonic processes as well as alteration forming phyllosilicate minerals. The exposures of crust available for investigation with orbital and landed measurements reflect these aggregate processes. The finding that much of the Noachian terrain on Mars exhibits evidence of phyllosilicate minerals and thus alteration [*Bibring et al.*, 2006; *Poulet et al.*, 2005; *Mustard et al.*, 2008] raises significant questions as to when, where, and how the alteration occurred. Furthermore, it is unknown how extensive and pervasive the alteration is, and whether any remnants of the early unaltered crust remain.

[3] One of the challenges in investigating this earliest period of Mars evolution is access to sections of the crust

[1]Department of Geological Sciences, Brown University, Providence, Rhode Island, USA.
[2]Johns Hopkins University Applied Physics Laboratory, Laurel, Maryland, USA.
[3]Institut d'Astrophysique Spatiale, Université Paris Sud, CNRS, Orsay, France.
[4]Laboratoire de Planétologie et Géodynamique, Université de Nantes, CNRS, Nantes, France.

0148-0227/09/2009JE003349

that show the geologic relationships among the key constituents that are also free of obscuring cover of dust, eolian material, or later volcanic and sedimentary deposits. A significant section of well-exposed Noachian crust exists surrounding the Isidis basin where remotely sensed data show strong mineralogic signatures of mafic silicates [*Hoefen et al.*, 2003; *Hamilton and Christensen*, 2005; *Mustard et al.*, 2005; *Tornabene et al.*, 2008] and phyllosilicates [*Bibring et al.*, 2006; *Poulet et al.*, 2005; *Mangold et al.*, 2007; *Mustard et al.*, 2008; *Ehlmann et al.*, 2009a, 2009b]. Importantly, the extent of mafic and hydrous mineral signatures can be clearly defined and can be linked to specific geologic and geomorphic units.

[4] The Isidis basin is a 1900 km [*Schultz and Frey*, 1990] diameter impact basin with a model age of Late Noachian (3.96 Ga) [*Werner*, 2005]. It has been significantly modified, including loss of the northeast rim through gradational processes [*Tanaka et al.*, 2002], formation of radial and concentric graben due to loading and flexure [*Wichman and Schultz*, 1989], and emplacement of the plains volcanics that make up Syrtis Major Planum on its western rim [*Hiesinger and Head*, 2004]. Flows associated with Syrtis Major extend from the central caldera to cover an area $\sim 10^6$ km^2. These flows reach the western floor of the Isidis basin, and cover the floor of the Nili Fossae trough. Early phases of the volcanism likely filled some of the Isidis basin floor [*Tornabene et al.*, 2008]. The opening of the fractures constituting the Nili Fossae as well as significant gradation due to fluvial processes [*Fassett and Head*, 2005; *Mangold et al.*, 2007] provide some excellent exposures of crust along scarp walls and in erosional windows. In these exposures outcrops are observed with spectral signatures diagnostic of mafic and phyllosilicate minerals.

[5] Previous analyses using data from past missions including Mars Global Surveyor, Mars Odyssey, and Mars Express have established the regional compositional, geologic, and geomorphic framework [*Hoefen et al.*, 2003; *Hamilton and Christensen*, 2005; *Mustard et al.*, 2007; *Mangold et al.*, 2007; *Tornabene et al.*, 2008]. Here we provide new analyses of high-resolution data sets from the Mars Reconnaissance Orbiter (MRO). Visible to near-infrared reflectance data from the Compact Reconnaissance Imaging Spectrometer for Mars (CRISM) [*Murchie et al.*, 2007a] are used to assess the character and distribution of units with Fe-bearing mafic silicates and hydrated silicates in the Noachian crust surrounding the Isidis basin. Imaging data with an average spatial resolution of 5 m/pixel from the Context Imager (CTX) [*Malin et al.*, 2007] define the regional morphologic context while the 25 cm/pixel imaging data from the High Resolution Imagine Science Experiment (HiRISE) [*McEwen et al.*, 2007] reveal detailed morphologic and stratigraphic characteristics.

2. Data Processing and Analysis

[6] The reduction of CRISM data from instrument units to atmospherically corrected surface reflectance involves several steps. The data are first converted to apparent I/F using procedures described by *Murchie et al.* [2007a]. Briefly, the detector background is subtracted using systematic measurements of the dark current that accompany Mars scene measurements. These dark-corrected data are then converted to radiance by dividing by measurements of the radiance emitted by an onboard integrating sphere and multiplied by a spectral model of the integrating sphere derived from ground calibrations. From these calibrated radiance data an estimate of I/F is generated by dividing by a solar spectrum. The solar spectrum is convolved to CRISM's wavelengths and resolution measured preflight and scaled to Mars' solar distance.

[7] These resulting I/F data contain the convolved signal of the surface and atmosphere. For the purposes of mineralogic analysis, it is important to remove the effects of the atmosphere. All the data used in this analysis were corrected using a simple multiplicative correction for the gas bands, but contributions from aerosols are ignored. The method was originally used in the analysis of ISM data [*Bibring et al.*, 1989] and continued in the analysis of OMEGA data [e.g., *Mustard et al.*, 2005]. A transmission spectrum of Mars is generated by CRISM observations over Olympus Mons (FFC000061C4). Many line averages over the base and top of the volcano are generated and the base average is ratioed to the top average. The ratio data are then scaled to 1.0 at 2.2435 μm. Assuming differences in reflectance from the surface at the two locations are negligible, this ratio provides the transmission spectrum for two passes through the atmospheric column between the summit and base of Olympus Mons. Because the CRISM detector has slightly different wavelength positions as a function of column position in the detector [*Murchie et al.*, 2007b], we generate a separate transmission spectrum for each column. This effectively samples the transmission of the atmosphere with the exact band passes of CRISM.

[8] From each CRISM spectrum the strength of the 2.011 μm CO_2 absorption is determined relative to a continuum defined by the spectrum's I/F outside the CO_2 absorption [*Pelkey et al.*, 2007; *McGuire et al.*, 2009]. The transmission spectrum from the same column position as the CRISM spectrum is then scaled to the observed CO_2 band strength and the CRISM spectrum is divided by the scaled transmission spectrum. Last, the observation is divided by the cosine of the incidence angle to generate apparent reflectance.

[9] This approach is generally effective at removing the dominant effects of the common atmospheric gases in the CRISM data. The lack of a correction of aerosols may affect overall spectral contrast (band strength) and long wavelength spectral shape or continuum properties. However, diagnostic narrow absorptions are not adversely affected and for data acquired with similar overall aerosol abundance to the Olympus Mons measurements the approach provides a reasonable first-order correction. A more rigorous assessment of atmospheric gases and aerosols can be derived using the full emission phase function data acquired with each CRISM targeted observation and applying radiative transfer algorithms such as DISORT [*Stamnes et al.*, 1988; *Arvidson et al.*, 2006].

[10] Mineral indicator parameters are calculated to guide analyses and provide summary products of spectral variance [*Pelkey et al.*, 2007]. The parameters were developed to capture the dominant modes of spectral variance related to mafic silicates, hydrated silicates, sulfates, and ices. They typically provide a standardized representation of absorption band strength and the full set of parameters for the CRISM

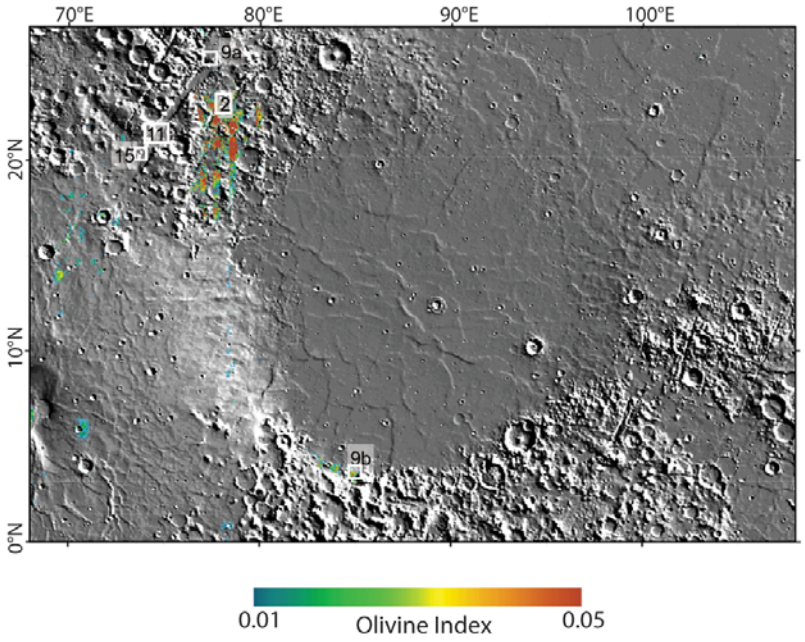

Figure 1. Regional view of the Isidis basin shown in MOLA shaded relief topography, overlain with an olivine mineral indicator map derived from OMEGA (color). The strength of the olivine signature varies from weak (blue) to strong (red). Locations of Figures 2, 9, 11, and 15 are shown with the white boxes and numbers.

investigation are provided by *Murchie et al.* [2007b]. All data were map projected using the line-of-sight intercept of each detector element with the MOLA shape model of Mars [*Murchie et al.*, 2007b].

[11] While mineral indicator parameters are useful guides, they can be equivocal and nonunique. For example, the index for the mineral olivine is designed to highlight regions with a broad absorption between 1.0 and 1.5 μm, and areas rich in olivine are readily identified by this parameter. However, other minerals with strong, broad absorptions in this spectral region (e.g., Fe-rich smectite clays) are similarly highlighted and the index value can be affected by strong spectral slope [*Salvatore et al.*, 2009]. Thus, regions of interest based on the mineral indicators/spectral parameters are systematically investigated in detail with spectral analysis to verify and validate the presence of mineral spectral signatures. This requires extraction of full spectral resolution data and comparison of these data to spectral libraries. To enhance the expression of spectral absorption features, we also employ ratioing techniques. The spectral data commonly exhibit artifacts due to errors in the removal of the atmosphere signal, and systematic instrumental errors [*Murchie et al.*, 2007a]. Many of these artifacts are common to all spectra, and are multiplicative in nature. Therefore, ratioing two spectra, where the numerator is extracted from an area of interest and the denominator from a region exhibiting a neutral or unremarkable spectral character, typically suppresses these artifacts. Due to the design of CRISM as a push broom array, many artifacts are associated along the columns of the detector, and therefore as columns in the CRISM imaging data. Thus in calculating ratios it is important that the numerator and denominator are extracted from the same column or columns in the case of area averages. Typically, we use at least 3 × 3 averages to increase the signal to noise in the resulting ratio spectra.

[12] Stereo HiRISE data were used to generate a digital elevation model using SOCET SET software. A mosaic of the red filter image data was generated. The left image was used as a control and features in the right image were matched to the left image. An automatic terrain extraction was then performed determining elevations by measuring X shifts in the rectified images. The resulting DEM is estimated to have a relative vertical accuracy of better than a meter. Some residual elevation spikes remaining were edited by hand to smooth the final product (R. Ollerenshaw, personal communication, 2008).

3. Results

[13] The general region of investigation is shown in Figure 1, with the distribution of olivine as determined by OMEGA overlain on the shaded relief image derived from MOLA data. The locations of specific observations described in this paper are shown by the white outlines. We have examined all the CRISM observations in this region and collectively they provide the fundamental results. However, it is not possible to present in detail all the observations and thus what we show here are the key observations that most clearly display the geologic relationships. The details of the spectroscopy of hydrous alteration minerals for the Nili Fossae region are described in the companion paper by *Ehlmann et al.* [2009a] and will not be repeated here. However, the same rigorous analyses are applied in arriving at the results and conclusions in this paper.

[14] The results are organized by an examination of the character of (1) the distinct olivine-bearing unit, (2) the nature of the basement rock, and (3) the properties of materials that

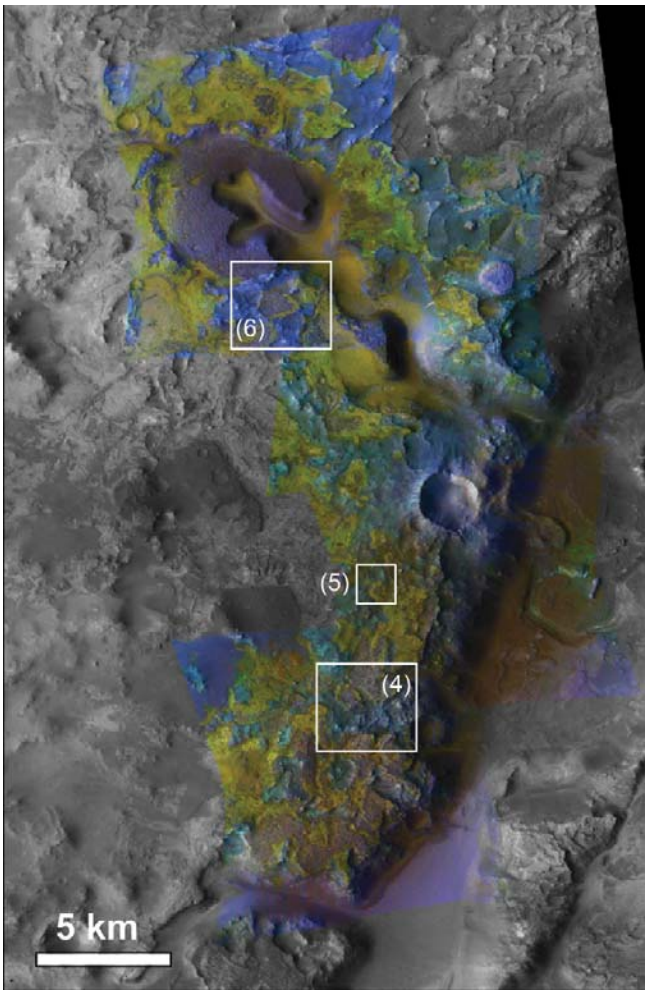

Figure 2. False color CRISM images FRT00003E12, FRT0000B438, FRT0000A4FC, and FRT0000871C (R, 2.38; G, 1.80; B, 1.15 μm) were used to colorize a portion of grayscale CTX image P03_002176_2024_XI_22N283W_070113. Olivine-rich surfaces appear yellow, phyllosilicate-bearing surfaces appear blue and turquoise, and the mafic cap unit is purple. High-resolution images from HiRISE data for the white boxes are shown in Figures 4, 5, and 6.

have filled large impact craters and troughs. We conclude by considering these observations in the context of the formation of the Isidis basin and subsequent events.

3.1. Olivine Stratigraphy

[15] A number of locations exhibiting strong olivine spectral signatures in TES [*Hoefen et al.*, 2003], THEMIS [*Hamilton and Christensen*, 2005; *Tornabene et al.*, 2008], and OMEGA [*Mustard et al.*, 2007] data have been observed with CRISM [*Mustard et al.*, 2008; *Ehlmann et al.*, 2008b] west and south of the Isidis basin (Figure 1). The olivine-bearing surfaces extend over a large region, much of which in the region east of Nili Fossae is covered by mobile materials and exhibits dune forms [*Hamilton and Christensen*, 2005]. However, at the resolutions of THEMIS and CRISM, bedrock outcrops are resolved. In particular, CRISM observations resolve the composition and morphology of three major units consistently associated with the olivine-bearing bedrock: a mafic caprock, a banded rock unit enriched in olivine, and phyllosilicate-bearing basement rocks (Figure 2). The spectroscopic signatures that define the key properties of the olivine bearing and the phyllosilicate units are shown in Figure 3. The olivine interpretation is based on the strong, broad 1 μm absorption. The width of this absorption is characteristic of high-Fe olivine such as fayalite; though large particle size and textural effects can also create such broad absorptions for forsteritic olivine. High Fe-olivine has also been reported for this region from TES [*Hoefen et al.*, 2003] and OMEGA [*Poulet et al.*, 2007] data. Fe/Mg-smectite clay is indicated by the presence of 1.4, 1.9 and 2.3 μm absorption bands (Figure 3) [*Ehlmann et al.*, 2009a], and this is the common phyllosilicate observed across Mars [*Poulet et al.*, 2005; *Mustard et al.*, 2008].

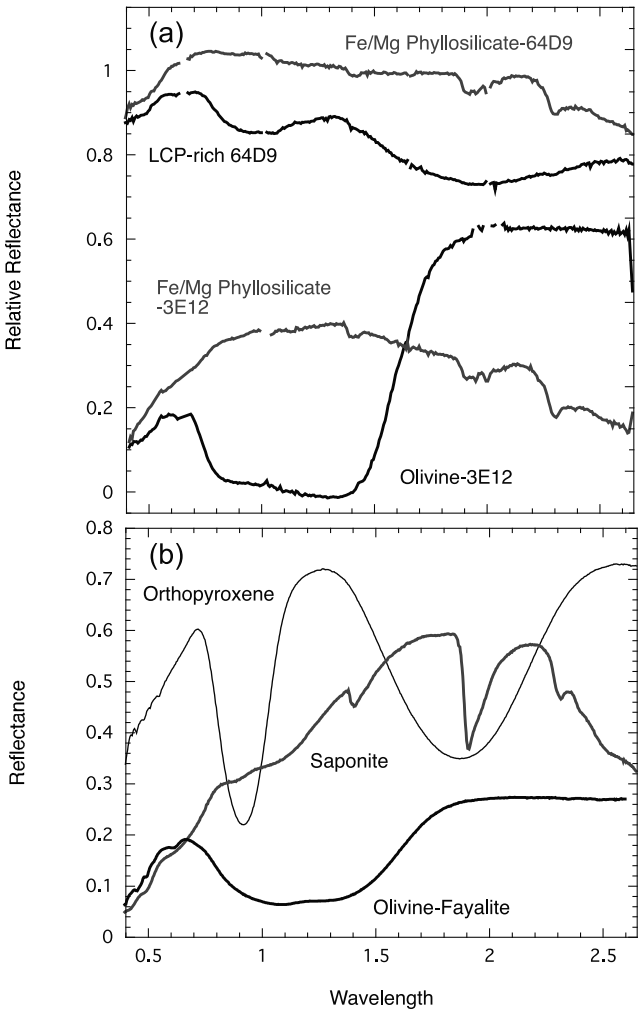

Figure 3. (a) CRISM and (b) laboratory reflectance spectra of key materials. Figure 3a shows CRISM relative reflectance spectra where the spectrum from a region identified by mineral indicator maps is divided by a spectrum of a region of spectrally unremarkable material. The key materials identified here are olivine-rich from CRISM observation FRT00003E12, low-Ca pyroxene–rich (LCP-rich) from FRT000064D9, and Fe/Mg-phyllosilicate-rich from FRT00003E12 and FRT000064D9. Figure 3b shows laboratory reflectance spectra of the pure mineral separates olivine-fayalite, orthopyroxene (LCP), and saponite (an Fe/Mg-phyllosilicate).

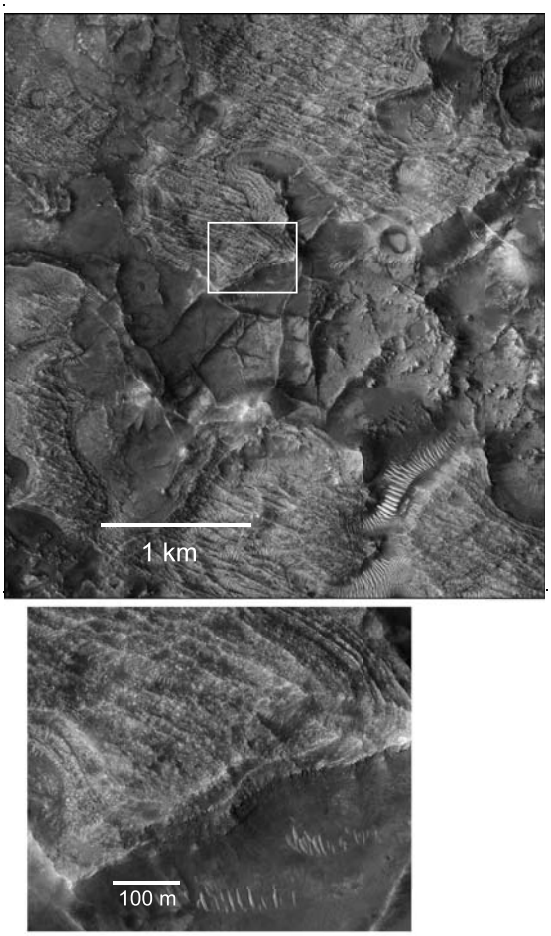

Figure 4. HiRISE image PSP_006712_2020. The textures and morphology of the mafic cap seen in Figure 2 have been removed by erosion, leaving a distinct corrugated eroded surface morphology and in some places exposing the underlying units. The contact between the banded olivine-bearing unit and the basement is clearly defined, and the banding is concentrated at the contact. The basement is strongly enriched in phyllosilicates with defined 1.41, 1.92, and 2.31 μm bands, indicative of an Mg-rich smectite clay. Linear ridges traverse the basement rocks intersecting at orthogonal angles. The ridges do not appear to penetrate into or disrupt the overlying olivine and cap units. The bright dunes in this region show strong signatures of olivine and are thus derived from the banded unit.

[16] The stratigraphy of a mafic cap overlying a banded olivine unit that in turn superposes the phyllosilicate-rich basement is observed over a large region of the Nili Fossae and along the southern rim of the Isidis basin. The geologic relationships are best defined in the central region of Nili Fossae shown in Figure 2. The association of a mafic cap poor in olivine overlying a more olivine-rich unit was also mapped in the southern region of the Isidis basin based on THEMIS data by *Tornabene et al.* [2008]. This region from Nili Fossae southeast to the Isidis basin floor materials was also investigated with OMEGA and HRSC data [*Mustard et al.*, 2007; *Mangold et al.*, 2007] where the general framework of the stratigraphy and nature of fluvial processes was defined.

[17] New data and observations from CRISM, CTX, and HiRISE data bring new perspectives and constraints on the evolution of this region. The mafic cap unit has a low apparent albedo with muted spectral signatures and exhibits a rough surface texture in high-resolution imaging (Figure 2). Where the cap unit is strongly eroded, a layered or banded unit is commonly observed at the base of the cap unit (Figure 4). We use the term ''banded'' because it is not clear from the available data whether these features are definitively layers, or another process such as cooling, shear deformation, or erosion has created an appearance of layering.

[18] The bands are variable in thickness but may be up to tens of meters thick and can be traced for hundreds of meters. The texture seen at highest resolution is fractured or blocky. Where erosion has almost completely removed the mafic cap and banded unit, olivine-bearing rocks can be seen filling low regions between linear ridges and appear to penetrate into fractures and dropped down sections (Figure 5). The banding appears to parallel the contact with the basement rocks (Figure 6) and drape the underlying topography defined by the phyllosilicate-bearing basement. In Figure 6b the banding is extremely well displayed in an erosional window where overlying units have been removed and the phyllosilicate basement has been eroded as well, forming a depression. The draping characteristics of the mafic cap and olivine units are best viewed with stereo HiRISE data. We generated a DEM using images PSP_002176_2025 and PSP_002888_2025 and drape the image PSP_002176_2025 over the DEM. A perspective view using these data shows that the olivine and mafic cap units clearly drape topography (Figure 7). The vertical bands may indicate the draping of the olivine over preexisting phyllosilicate basement rock, which since has

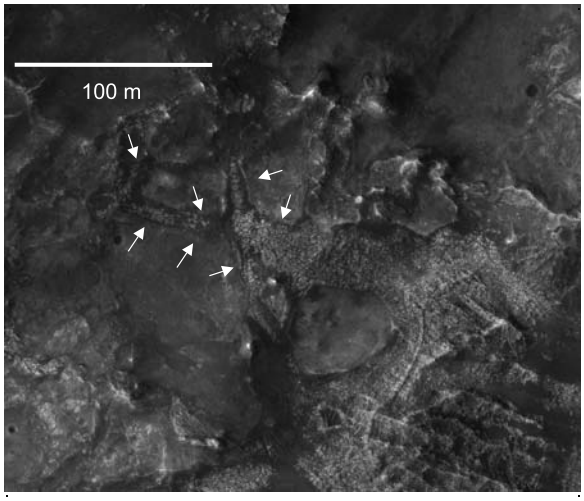

Figure 5. HiRISE image PSP_006712_2020. The white arrows point to olivine-rich rocks in contact with the phyllosilicate basement. At high resolution, the olivine-bearing unit is polygonally fractured and fills low regions between linear ridges and penetrates into down-dropped sections as shown by the regions highlighted by the white arrows.

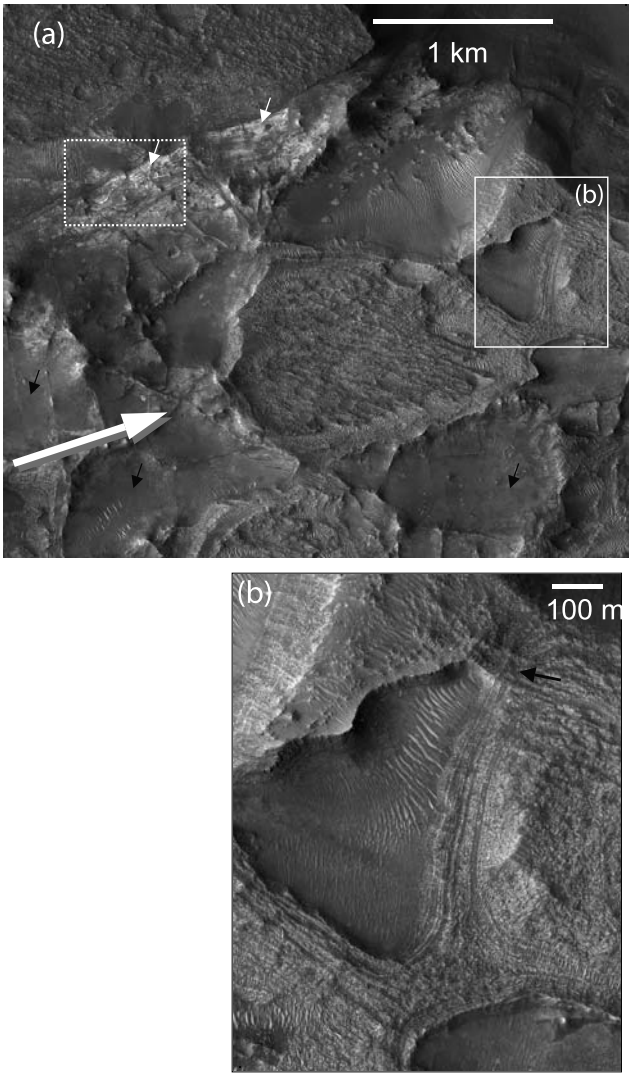

Figure 6. (a) HiRISE image PSP_002176_2025. Well-preserved mafic cap in the northwest corner of this image overlies the banded unit that rests directly on the phyllosilicate-bearing basement. The phyllosilicate basement is itself banded or layered in places shown by the small white arrows and massive in others, shown by the black arrows. Linear ridges are clearly seen within the phyllosilicate-bearing rocks in the western third of the image. (b) The enlargement shown by the white box shows well-defined banding contouring an erosional window through the cap and olivine-bearing unit. Toward the upper portion of the enlargement, the banding is seen to be oriented vertically (black arrow). The view direction for the perspective view shown in Figure 7 is shown by the large white arrow. The dotted white box shows the location of Figure 8.

been preferentially removed by erosion, or could be the result of deformation of the region by folding.

[19] The very strong, broad olivine absorption between 1.0 and 1.5 μm shown by the olivine-bearing unit (Figure 3) is consistent with the OMEGA observations at lower spatial resolution [*Mustard et al.*, 2007]. No other mafic mineral absorptions are observed in the banded unit, although alteration minerals (e.g., magnesium carbonate) associated with the banded unit indicate partial in situ aqueous alteration of olivine [*Mangold et al.*, 2007; *Ehlmann et al.*, 2008b, 2009a, 2009b]. The character and extent of alteration (partial to complete) varies spatially, and numerous unaltered olivine bedrock units persist. In these, there is a noticeable increase in the strength of the olivine absorptions around the edges of the eroding cap, where the massive mafic caprock is largely removed and where nighttime THEMIS data show a high temperature implying rocky or more indurated surfaces. The cap unit itself exhibits a weak olivine spectral signature. That very strong olivine signatures result where the banded unit is best exposed indicates that the olivine signature is in the rock unit and not simply in a mobile component such as the dunes (Figures 2, 4, and 6), and the association of olivine signatures with regions of higher thermal inertia has been noted by others [e.g., *Hamilton and Christensen*, 2005; *Tornabene et al.*, 2008]. The contact between the spectrally bland mafic cap and banded olivine unit (sharp versus diffuse or gradational) is not resolved even at HiRISE resolution.

[20] In contrast, the contact between the olivine-rich banded unit and the underlying unit interpreted to be Noachian basement crust is sharp (Figures 4, 6, and 7). In this region the Noachian basement exhibits spectral signatures diagnostic of Fe/Mg-smectite clays. This Noachian crust, exposed by erosion, typically exhibits a smooth surface texture. Distinct layering or banding is observed in some regions (Figures 4 and 6), indicated by differences in tonality or brightness. In addition to the layering, breccia blocks are observed throughout the region. The examples shown in Figure 8 show the blocks range in size from tens to hundreds of meters and blocks of similar character in Noachian crust have been seen elsewhere [*McEwen et al.*, 2008]. The density of blocks varies from high, where the blocks appear to be in contact with one another, to low, where they are infrequent and within a massive matrix (Figure 8). The exposures are not good enough to define the size of the largest blocks, but the phyllosilicate material that shows a banding and is in contact with the overlying olivine-bearing unit seen in Figure 8 may be a portion of one large breccia block that is over a kilometer in length.

[21] Raised, linear features several meters in width and many hundreds of meters in length are observed in the clay-bearing basement (Figures 4 and 6). These ridges are observed over a large area including all the area encompassed in Figure 2 and the region to the north of Figure 2. The linear features traverse the phyllosilicate-bearing basement frequently intersecting at orthogonal angles and the density varies from sparse or absent to frequent. Where these features emerge next to the overlying olivine-bearing unit, there is neither evidence of deformation in the overlying units due to the linear features nor evidence of linear features with the same orientation in the overlying mafic igneous units. This demonstrates that the linear features predate emplacement of the olivine-bearing unit. The linear features are more resistant to erosion than surrounding materials, resulting in their raised appearance.

[22] Where well exposed, the contact between the phyllosilicate-bearing basement units with the overlying olivine-bearing banded unit is sharp. In HiRISE IRB color imagery, unaltered olivine-rich rocks are a distinctive blue/turquoise color while phyllosilicate-bearing rocks are brown and this contact is sharp at the resolution of HiRISE. At CRISM

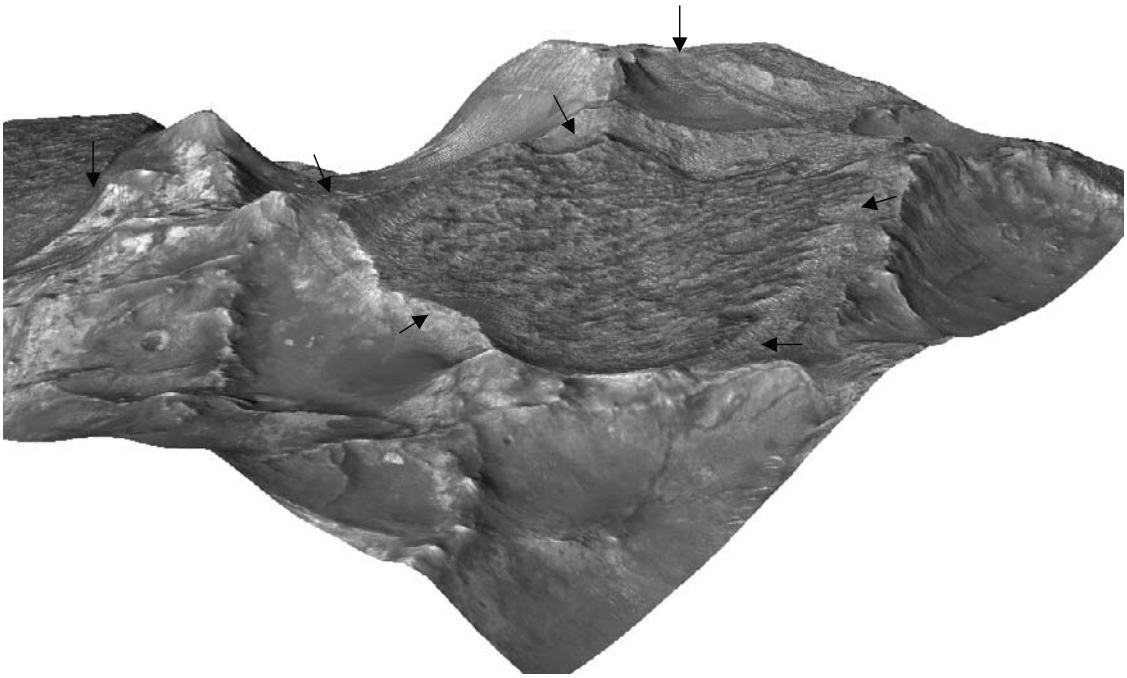

Figure 7. Perspective view of HiRISE image PSP_002176_2025 draped over a HiRISE digital elevation model constructed with the stereo pair PSP_002176_2025 and PSP_002888_2025. Black arrows highlight outcrops of the banded olivine-bearing unit (see also these locations in Figure 6). It is clear this unit drapes the topography, and the banding is generally parallel to the contact with the substrate. Vertical exaggeration is 5X.

resolution there are regions showing gradational or diffuse transitions in the mineral indicator maps (Figure 2). High-resolution imaging shows that these areas commonly have mobile materials present in the form of dunes (Figures 2, 4, and 6), leading to diffuse spectral signatures at the contact. But where the contacts are cleanly exposed, the mineral indictor maps show sharp, crisp boundaries.

[23] An olivine-rich unit beneath mafic caprock and together resting on phyllosilicate-bearing basement is observed extensively in the region 20°–23°N and 77°–80°E where banding in the olivine unit is generally well defined. This stratigraphy is also observed north and west of the Nili Fossae trough at 24°N, 76°E in CRISM observation FRT00008389 and along the south edge of the Isidis basin in Libya Montes in CRISM observation HRS000047D8 (3°N, 85°E, Figure 9) associated with Hashir crater. This area was also examined in detail by *Tornabene et al.* [2008] with THEMIS data. Layered or banded morphologies are apparent in HiRISE image PSP_002822_1830 associated with CRISM observation HRS000047D8 (Figure 9). Erosion has created a window through the mafic cap and olivine units to the phyllosilicate basement that reveals the same characteristic stratigraphy also observed around Nili Fossae (e.g., Figure 2). While banding in the olivine-bearing unit is not as well defined or exposed as elsewhere (e.g., Figures 2 and 4) a HiRISE stereo pair associated with this observation (PSP_002756_1830) shows the banding dips away from the central mound (Figure 10). There is a strong olivine mineral signature in the materials exposed at the base of the material that fills this crater. This is particularly well exposed in the moat along the west and north area of the crater floor in the CRISM image shown in Figure 9. These olivine-rich lithologies have the same signatures as the material that is in contact with the phyllosilicate-bearing central mound. The central mound is probably the structural uplift of the crater forming the central peak. Thus, the olivine-bearing unit is found on the floor of the crater as well as tilted up in contact with the structural uplift. While the mafic cap and olivine-bearing units fill the floor of the crater and are tilted up around the central mound, they do not reach as high as the crater rim, and there is no evidence that crater fill constituting the olivine/mafic cap ever breached the crater rim.

[24] The timing of emplacement of the olivine-bearing unit with respect to the formation of the fossae is well defined in the Nili Fossae area. The olivine unit with the mafic cap is cut by the fractures that form the Nili Fossae and traverse the study area (Figures 4 and 9). In Figure 4, there is a fracture running along the eastern edge of the scene. The olivine unit is found on the upland plateau material right up the edge of the fracture but not draped over the walls. The olivine unit is not seen on the floor of the fracture, although the floor of the fracture has been filled by sediments (layered rocks) and mobile material. Better exposure is provided to the northeast, where two fractures intersect (Figure 9c). The fractures clearly truncate the olivine and mafic caprock units; eroded olivine-bearing sands fill the fracture floors. This indicates the fractures postdate the olivine unit and mafic cap. The plateau throughout this region shows a strong olivine spectral signature beneath a thin mafic cap that was observed with OMEGA data [*Mustard et al.*, 2007; *Mangold et al.*, 2007]

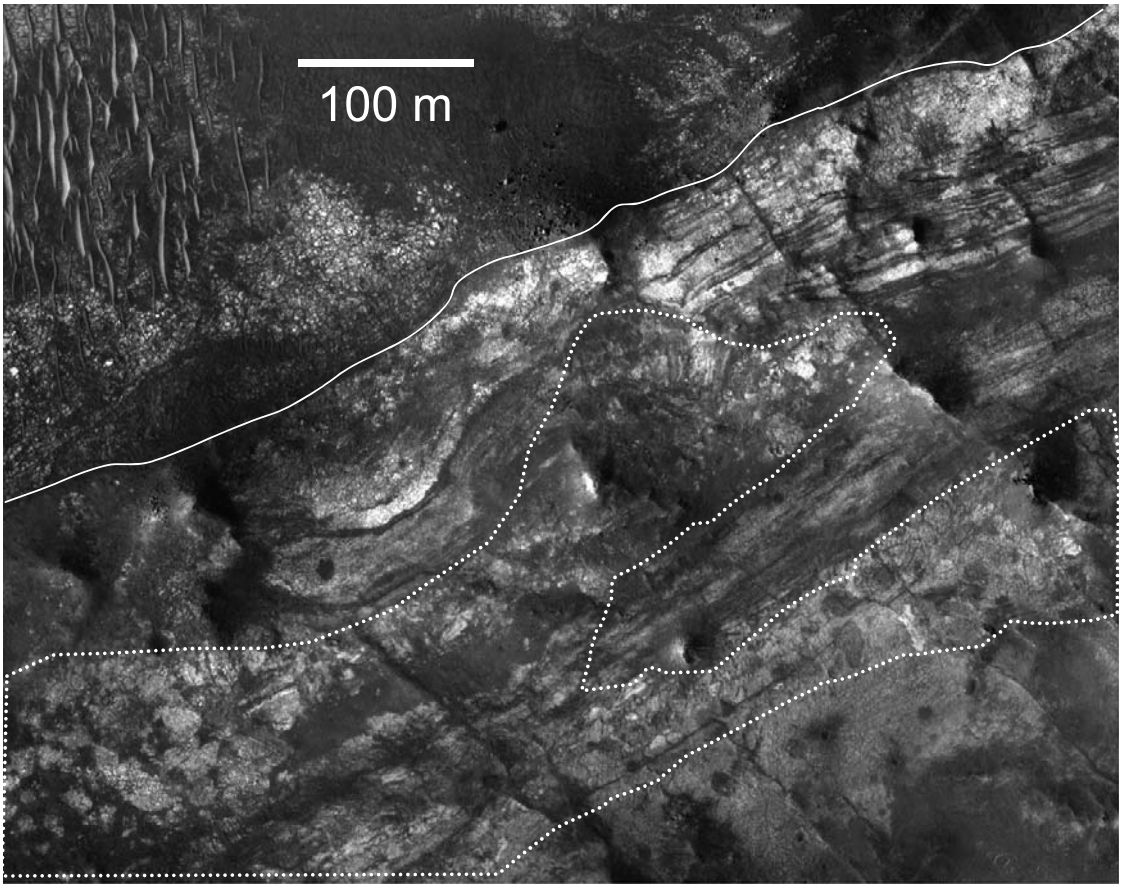

Figure 8. Section of HiRISE image PSP_002176_2025 at the contact between the mafic cap/olivine unit and phyllosilicate basement. The approximate location of the contact is shown by the solid white line. In the phyllosilicate basement, banding or layering is clearly seen close to the contact. This layering shows gentle folding and offsets along fractures. The dotted white polygon outlines a region of large breccia blocks, tens of meters in size. In the southeast of the scene (bottom right) there is an absence of layering and a more sparse population of breccia blocks.

but the MRO data has clearly resolved the details of the stratigraphy and the timing of the emplacement of the olivine as definitively prefossae formation.

3.2. Basement Crust: Character and Composition

[25] Exposures of bedrock along the Nili Fossae trough, in impact craters, and in areas of deep erosion provide a window into the Noachian basement crust in this region. The crust shows a diversity of compositions, ranging from unaltered lithologies spectrally dominated by the mafic silicates olivine, low-Ca pyroxene (Figure 3), and high-Ca pyroxene to regions where spectral signatures are dominated by phyllosilicates and mafic minerals are not apparent. In both regions, other mineral phases are likely present, but their spectral signatures in the near infrared are not distinctly resolved. In orbital thermal infrared data, phyllosilicate-rich regions in Nili Fossae appear to be dominated by basaltic constituents [*Michalski et al.*, 2009]. This indicates that while alteration is widespread it may not pervasive. Modeling by *Michalski et al.* [2009] suggests 15–30% phyllosilicate in the exposures large enough to be resolved by the Thermal Emission Spectrometer (3 × 6 km per pixel). Geological relationships of lithologic units in the Noachian crust are described below.

[26] In a few regions covered by CRISM and HiRISE observations the exposures are sufficiently free of obscuring dust, talus, or eolian material to resolve the relationships between the components of Noachian-aged bedrock basement. This is superbly shown in the central region of the Nili Fossae trough where tectonic forces and erosion have combined to expose a thick section of Noachan crust (Figure 11). This site was considered as a possible landing site for the Mars Science Laboratory and has been extensively covered by HiRISE, CTX, and CRISM. The region is on the edge of the Nili Fossae trough where a reentrant, formed by sapping processes, emerges from the east. The scarp walls are 400–600 m high (Figure 12). The floor of Nili Fossae is covered by Hesperian lavas from Syrtis Major [*Hiesinger and Head*, 2004] and partially by ejecta from the 65 km diameter Hargraves crater located 50 km to the east of the fossae. Topographic profiles across the fossae show that the ejecta is approximately 250 m at its thickest (Figure 12). CRISM mineralogic mapping and HiRISE data show that the ejecta from Hargraves crater is a mélange of phyllosilicate and mafic blocks in a matrix of phyllosilicate-dominated material (Figure 11). The Hesperian lavas show spectral properties consistent with those in Syrtis Major, dominated by HCP, with minor LCP and olivine [*Skok et al.*, 2009]. The scarp

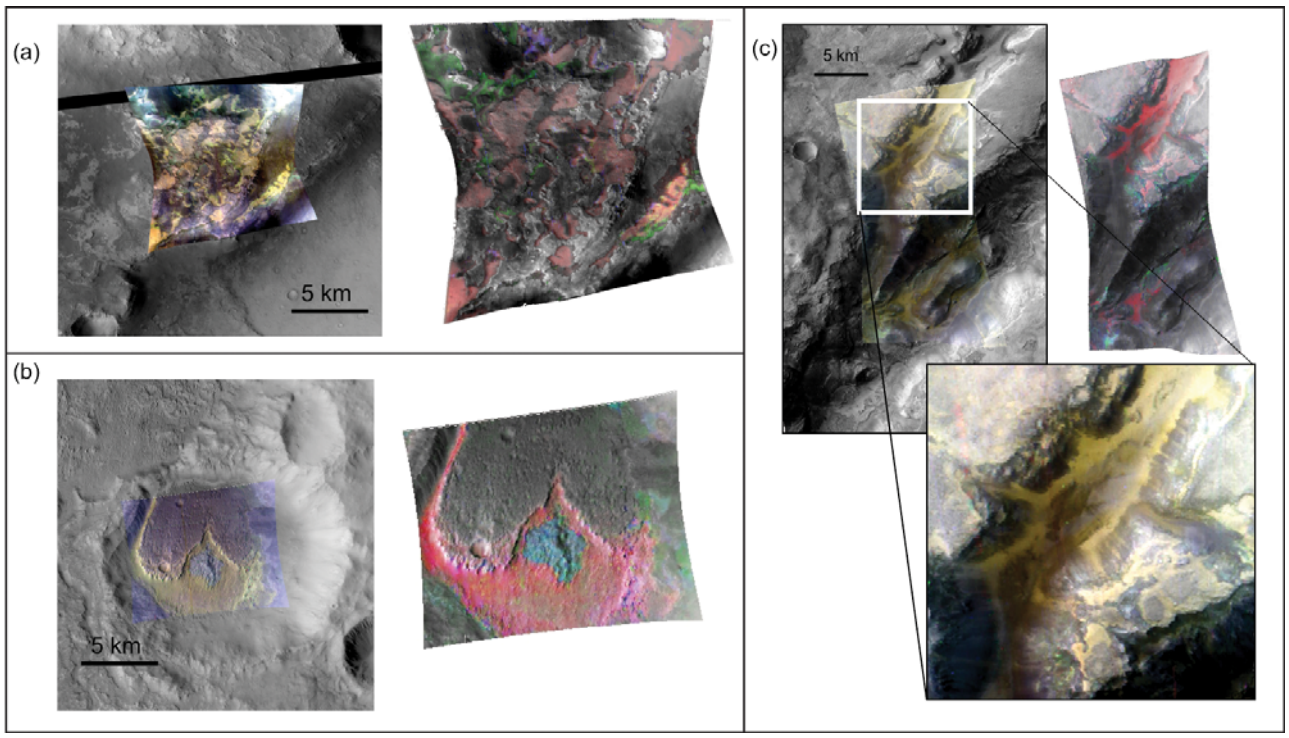

Figure 9. Color composites and mineral indicator maps of CRISM observations FRT00008389, HRS000047D8, and HRL0000B6FF. In the color composites olivine-rich surfaces appear yellow/gold, while in the mineral indicator maps the colors correspond to the specific mineral indictors used. (a) Infrared color composite of FRT00008389 (left; R, 2.42; G, 1.81; B, 1.08). Mineral indicator maps for olivine (right); 1900 nm absorption (red) and 2300 nm absorption (green) merged with infrared albedo at 1.3 μm for image FRT00008389 (blue). (b) Infrared color composite of HRS000047D8 (left; R, 2.42; G, 1.81; B, 1.08). Mineral indicator maps for olivine (right); 1900 nm absorption (red) and 2300 nm absorption (green) merged with infrared albedo at 1.3 μm for image (blue). (c) Infrared color composite of FRT0000B6FF (left; R, 2.42; G, 1.81; B, 1.08). Mineral indicator maps for olivine (right); 1900 nm absorption (red) and 2300 nm absorption (green) merged with infrared albedo at 1.3 μm for image FRT0000B6FF (blue). (Bottom, right) Enlargement of the central part of the color composite that clearly shows the olivine strata in the central region cut and truncated by fractures of the fossae.

walls are dominated by the spectral signatures of Fe/Mg-phyllosilicate (Figure 3) while the plateau is heterogeneous but dominated by signatures of mafic silicates.

[27] We have merged CRISM mineral indicator maps derived from observation FRT000064D9 with HiRISE image PSP_003086_2015 (Figure 13). In this merged product, the spectral signatures of mafic silicates are strongly expressed in some breccia blocks. A clear example if this is shown in Figure 3 where the spectrum from an LCP-rich breccia block is shown. In the scarp faces as well as along the floor of the trough, breccia blocks tens to hundreds of meters in size are exposed. Many blocks are phyllosilicate bearing, showing absorptions near 1.9 and 2.3 μm, typical of Fe/Mg-smectite clays (Figure 3). Some of the breccia blocks here and elsewhere show banding suggestive of layering (Figure 14) as was also described for breccia blocks in Figure 8. Other blocks are massive and apparently of more uniform texture and composition. In color HiRISE data [*Delamere et al.*, 2009] with wavelengths at infrared ($\sim$0.7–1.0 μm), red ($\sim$0.5–0.9 μm), and blue-green ($\sim$0.4–0.6 μm) wavelengths displayed as RGB, blocks rich in mafic silicates typically express a blue-green color (Figure 13). We have confirmed with spectral signatures from CRISM data that these blocks are dominated by pyroxene absorptions and are relatively enriched in LCP. Several blocks exposed in this observation are partly unaltered and partly altered, suggesting the presence of an alteration front (Figure 13c).

[28] Relationships between unaltered and altered rock are also well expressed in observation FRT00009D44 that covers the eastern scarp of Nili Fossae, upper plateau, and Hesperian-aged lava along the floor of the trough (Figure 15). CRISM data show the scarp face is strongly enriched in Fe/Mg-smectite clay, and the floor of the trough shows mafic signatures enriched in olivine and HCP, comparable to mineral signatures of the broader Syrtis Major region [*Skok et al.*, 2009]. The composition of the plateau is mottled, with the different mineral signatures associated with specific patches or regions dominated by LCP-rich mafic silicates or alternatively phyllosilicate (1.9 and 2.3 μm), and the edges of the regions are defined by diffuse boundaries.

[29] In color HiRISE data (PSP_007200_2005) crossing the plateau and scarp, weakly to unaltered LCP-rich rocks are a distinct aquamarine color and the phyllosilicate-bearing matrix is brown. On the plateau, regions of LCP-dominated terrains define distinct but irregular patches. At the top of the scarp face these same rocks are sometimes beautifully

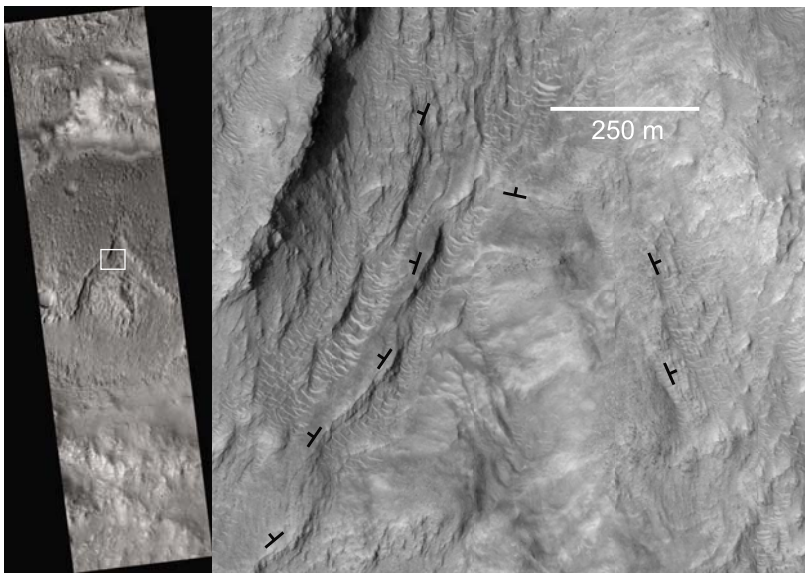

Figure 10. (left) HiRISE image PSP_002822_1830. Image width is approximately 6 km. (right) Enlargement of the white box shown on the left. The black lines with the small orthogonal line midway define the approximate strike and direction of dip for layering draped over the central mound of this crater.

exposed as definite bands of unaltered rock, meters thick, embedded in a matrix exhibiting a strong phyllosilicate spectral signature. The bands or layers of LCP-rich rock are of variable thickness and can be traced for tens to hundreds of meters but are nonetheless discontinuous, and show evidence of folding (Figure 15). The brown phyllosilicate materials are intimately interleaved with the LCP-rich rock. Lower on the scarp are phyllosilicate-bearing breccia blocks that exhibit finely banded or layered properties (Figure 15).

3.3. Transport and Fill

[30] There is abundant evidence for large-scale transport and deposition of sediments and lavas following the Isidis impact event and the opening of the fossae. This is illustrated by the stratigraphy of successive units of fill that have been exposed in the Nili Fossae trough, the widest of the fossae (Figures 11 and 15). CRISM data show the uppermost unit in the trough consists of over 250 m of phyllosilicate-bearing ejecta from Hargraves crater that has been emplaced on lavas that flowed into the Nili Fossae trough from Syrtis Major (Figure 12). Along the profile of Figure 12, the lavas are exposed beneath the ejecta in a 5–10 km wide strip along the western edge of the trough. In contrast, to the north and south of the Hargraves ejecta the volcanics are continuously exposed across the full 30 km width of the trough. Along the western edge of the trough the volcanics embay phyllosilicate-bearing rocks that apparently continue beneath the volcanics. This is illustrated in Figure 13 where the gray Hesperian lavas are observed in the southeast corner of the scene embaying the light magenta trough floor material. The light magenta trough floor material contains distinct Fe/Mg-smectite clay absorption features and shows crude bedding or layering. Moving to the northwest there is an erosional moat around a 500 m tall mesa capped with LCP-enriched rocks (Figure 13). The trough fill seen in the moat shows meter-scale polygonal fracturing at the highest resolution and the erosion has exposed crude layering in the bedrock. The trough fill shows weak absorptions at 1.9 and 2.3 μm due to the presence of Fe/Mg-phyllosilicate. These absorptions are weaker but of the same general character as those expressed in the scarp faces. The scarp faces show a different erosional style of a uniform, massive unit that does not show blocks or polygonal fracturing. A generalized cross section of the key units described above is shown in Figure 16.

Figure 11. (a) Regional THEMIS daytime IR image mosaic of the area centered around Hargraves crater. The center of Hargraves is shown by the black arrow, and the ejecta from Hargraves extends to the floor of the Nili Fossae trough running southwest-northeast across the western third of the image. Other fractures with a similar orientation are to the west of east of Nili Fossae, one of which is covered in Figures 2 and 9. The floor of Nili Fossae is veneered by lava from the Syrtis Major volcanic complex to the southeast, and the ejecta from Hargraves superposes the lava flows. The locations of Figures 2, 9, and 11b are shown by the white boxes and numbers. The black lines terminated by solid circles show the locations of the MOLA topographic profiles shown in Figure 12. (b) Mineralogy indicators of CRISM observations for 1900 nm hydration absorption (blue), broad ferrous absorptions between 1 and 1.6 μm (red), and low-Ca pyroxene (green) merged with CTX images. Mineral indicators are calculated using the methods of *Pelkey et al.* [2007]. The legend provides an interpretation of the color to mineralogy. The main Nili Fossae trough runs southwest to northeast in this mosaic, and the western wall of the scarp is ~400–600 m in height (see Figure 12). The white box shows the location of Figure 13. CRISM images used are FRT000064D9, FRT00007BC8, FRT00008530, FRT0000A4B5, and FRT0000B012. CTX images are P05_003086_2011, P07_003587_2005, P14_006488_2006, and P15_006989_2022. The mosaic is centered at 21.1°N and 74.4°E.

[31] There are a number of craters in this region that are partially filled. A small crater located at 20.6°N, 73.8°E is cut by the western scarp and associated erosion of the Nili Fossae trough (Figure 17). The rim of this 6 km diameter crater is indistinct from the combination of sedimentary fill and erosion, but the circular border around the fill materials is unmistakable. The fill is composed of sediments layered at a scale of meters to tens of meters that show strong absorptions due to Fe/Mg-phyllosilicate (Figure 17). *Ehlmann et al.* [2009a] describe a larger 40 km diameter crater located northwest of Figure 11 at 22.4°N, 74.2°E with approximately 1 km of fill dominated by Fe/Mg-smectite clays. Near the top of the fill is a distinctive layer with absorption features diagnostic of kaolinite. As described by *Ehlmann et al.* [2009a], this distinctive kaolinite layer is apparently a regional unit. Where undisturbed by impact or erosional

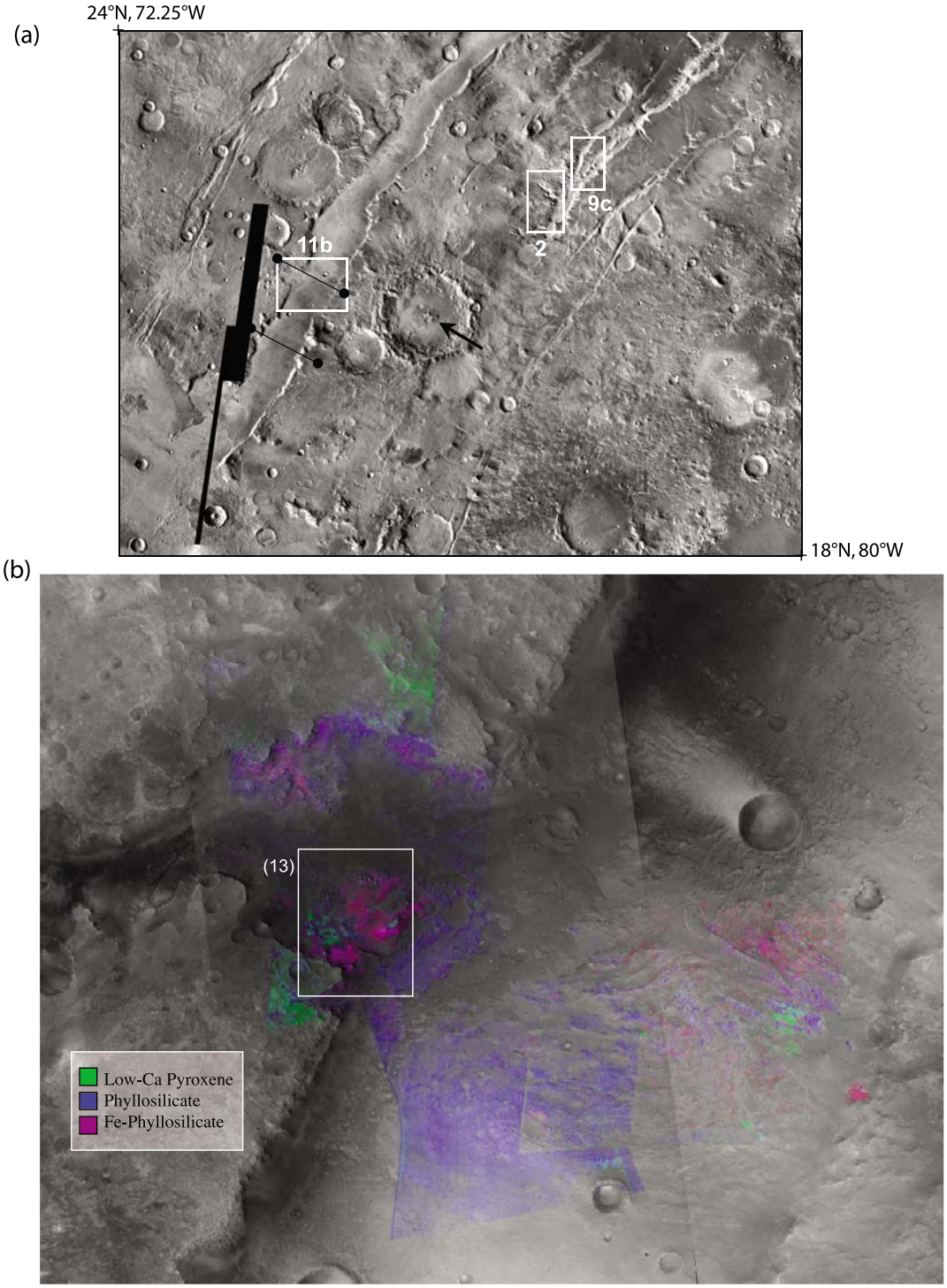

Figure 11

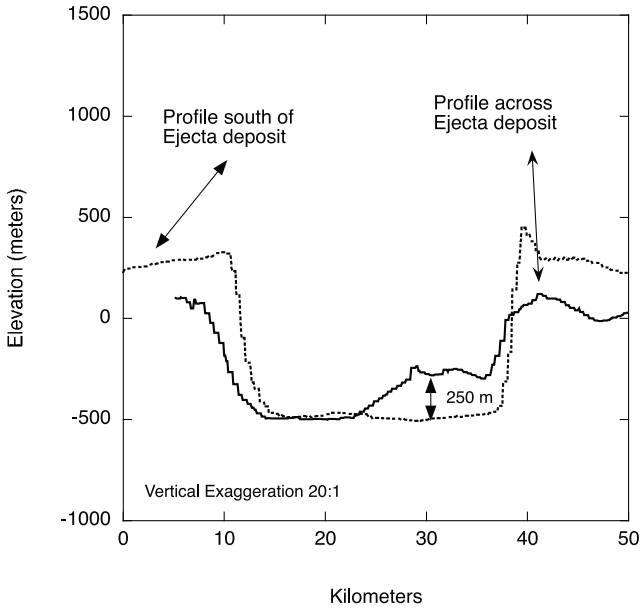

Figure 12. Topographic profiles across Nili Fossae trough south of the ejecta of Hargraves crater (dotted line) and across the ejecta from Hargraves crater (solid line).

processes, the deposit is typically thin and rests several tens of meters below the surface beneath a spectrally unremarkable mantling unit. The kaolinite is found above both sedimentary Fe/Mg-phyllosilicate fill and on the plateau. Like the sedimentary Fe/Mg-phyllosilicates in Figure 17, faulting cuts the kaolinite layer and erosion associated with the formation of the Nili Fossae trough.

[32] The presence of phyllosilicate-bearing, compositionally distinct fill material in impact craters and in the trough underlying Hesperian lava indicates that there was a significant period of gradation both prior to and subsequent to the Isidis basin formation and the opening of the Nili Fossae fractures. That process had largely ceased by the time of the emplacement of the Hesperian lava as there are few deposits of this nature that superpose the Hesperian lavas [*Mangold et al.*, 2008]. Fluvial channels including sapping landforms debouche into the troughs and craters (Figures 2 and 11) and may have been the pathway by which sediment was delivered to form the sedimentary fill deposits [*Mangold et al.*, 2007; *Ehlmann et al.*, 2008a, 2009a]. At CRISM resolution, it is apparent that many of the fill materials are phyllosilicate-bearing and are most likely materials transported from the adjacent, strongly altered Noachian crust.

4. Discussion

[33] The high-resolution data from the Mars Reconnaissance Orbiter provide new insight into the stratigraphic and

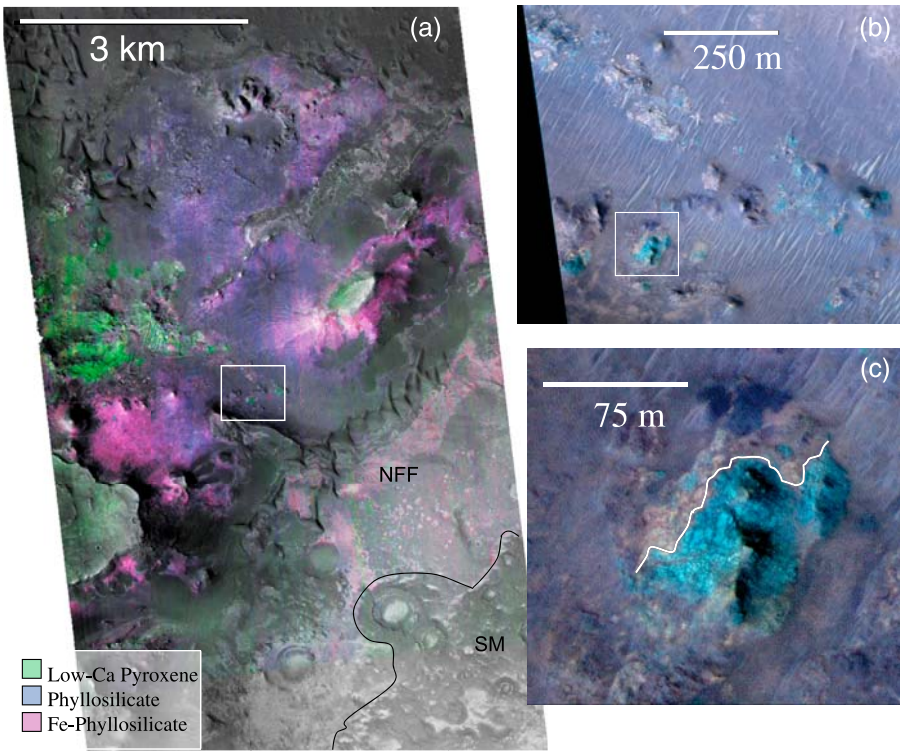

Figure 13. (a) Same mineral indicators as shown in Figure 11 merged with HiRISE image PSP_003086_2015. CRISM image used to generate the mineral indicators is FRT000064D9. The white box shows the location of Figure 13b. (b) Color HiRISE image PSP_003086_2015 shown with the infrared filter in red, red filter in green, and blue filter in blue. Unaltered LCP-rich rocks appear turquoise/green. The white box here shows the location of Figure 13c. (c) Full-resolution enlargement of HiRISE IRB color image.

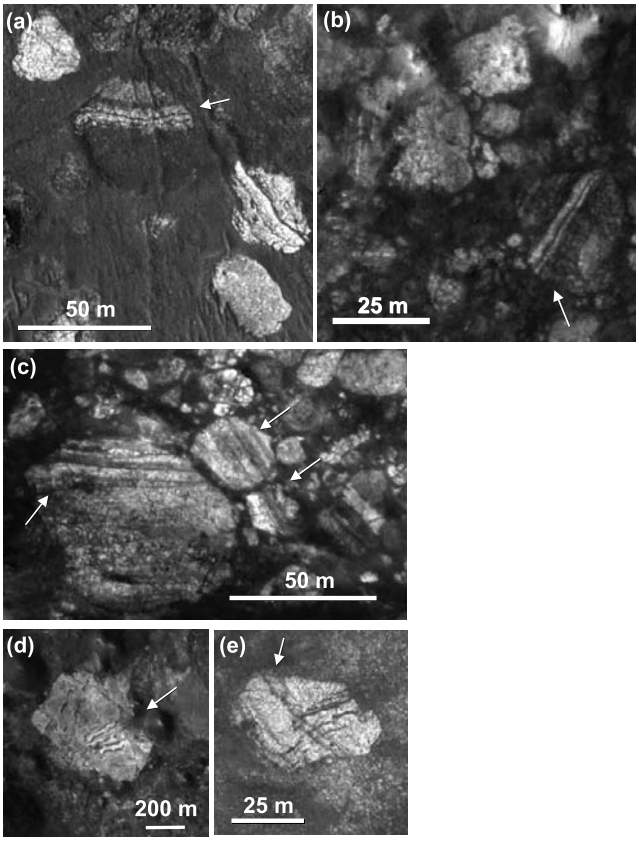

Figure 14. Breccia blocks with meter-scale layering within basement rocks in Nili Fossae. HiRISE images are from subsets of (a) PSP_002176_2075, (b) PSP_007569_2020, (c) PSP_006923_1995, (d) PSP_3086_2015, and (e) PSP_2176_2075.

geologic relationships of Noachain-aged units in the Isidis basin region. The deeper sections of Noachian crust exposed in strongly eroded terrains or along scarp walls are complex, showing no evidence for an assemblage of units that define a coherent stratigraphy. Instead the crust that is exposed and that we can observe is apparently a breccia consisting of material ranging in size from fragments that are smaller than the finest resolution of MRO (25 cm/pixel, HiRISE), to blocks many hundreds of meters to kilometers in size. The density of blocks is also highly variable from regions in which no breccia blocks are resolved to those in which the breccia blocks are in direct contact with each other (Figures 4 and 8).

[34] The compositions and textures of blocks and matrix material in the breccia are highly diverse. The CRISM near-infrared data show mineral compositions ranging from unaltered mafic silicate lithologies to regions that are dominated by Fe/Mg-smectite clay that show little evidence for other mineral constituents. Thermal infrared data suggest the alteration is 15–30% with the bulk of the rock composed of basaltic minerals, but the Thermal Emission Spectrometer spatial resolution cannot resolve individual outcrops of basement crust exposed at the CRISM scale. In some regions it appears that a phyllosilicate matrix envelops unaltered mafic-silicate blocks, while other regions show large blocks that are composed of both altered and unaltered material (Figure 13). Clear banding from fine to coarse scales can be observed in many breccia blocks (Figure 14). This is different than the banding observed in the scarp of Nili Fossae as shown in Figure 15. The origin of the fine banding in some breccia blocks is not clear, but likely includes lacustrine, fluvial, and eolian processes as well as possibly volcanic (e.g., ashfall) or impact processes. Regardless it is clear that the banded or layered structures were formed and lithified prior to the process that created the large, coherent breccia blocks.

[35] The Isidis basin is highly degraded [*Tanaka et al.*, 2002] with the northeastern rim removed and covered by deposits of the northern plains and the west rim by the volcanics of Syrtis Major planum [*Hiesinger and Head*, 2004]. However, the brecciated basement exposures characterized by Figure 8 are located between the putative transient cavity of the Isidis impact and the final rim of the crater. The deposits exposed along the walls of the Nili Fossae trough (Figure 15) are in the region proposed to be the rim [*Werner*, 2005; *Schultz and Frey*, 1990]. The breccias near the rim may be ejecta from the Isidis event, while those exposures deeper in the basin (Figure 8) may be fractured and brecciated pre-Isidis crust, or fall back breccia from the impact. If fluvial and lacustrine processes formed the fine-scale horizontal layering found in some breccia blocks, these blocks preserve evidence for extensive hydrologic processes on early Mars.

[36] In addition to breccia blocks, raised linear ridges are commonly observed in the Noachian basement exposed in the Nili Fossae region. These raised, linear features are similar to structures observed in a number of craters in the Nili Fossae region that *Head and Mustard* [2006] interpreted to be breccia dikes. Clasts or breccia fragments are not observed associated with the linear ridges at HiRISE spatial resolution. While no clasts are observed, dust or particulate cover may obscure them. In addition to breccia dikes, the linear features may be the result of fractures in the basement rocks that were conduits of fluid flow that became mineralized as suggested by *Mangold et al.* [2007]. CRISM data do not show these features to have a different composition than the surrounding rocks. However, the mineralizing cement may not be mineralogically distinct from the surrounding rocks or may not have an infrared active mineralogic signature. The linear features could be magmatic dikes intruded by igneous processes. In this case mafic igneous mineralogic signatures would be expected and/or evidence of contact metamorphism with the surrounding phyllosilicate-bearing rocks. These properties are not observed. The presence of the linear raised features indicate a process that lithified or cemented the phyllosilicate-bearing Noachian crust. The resulting cemented zones are arranged as if a network of fractures that could have served as conduits for fluid flow. The generation of the fractures as well as stimulation of fluid flow may have been related to the Isidis basin–forming event or could have predated the basin.

[37] The character of the banded olivine unit is well defined by the new MRO observations. It is olivine-rich, in direct contact with brecciated phyllosilicate-bearing basement rocks. The olivine-rich bands are superposed by a more massive mafic caprock above that has weak to absent olivine spectral signatures. The banding parallels the contact with phyllosilicate basement in most places, conforming to topography (Figures 4, 6, 7, 9, and 10). We interpret the strati-

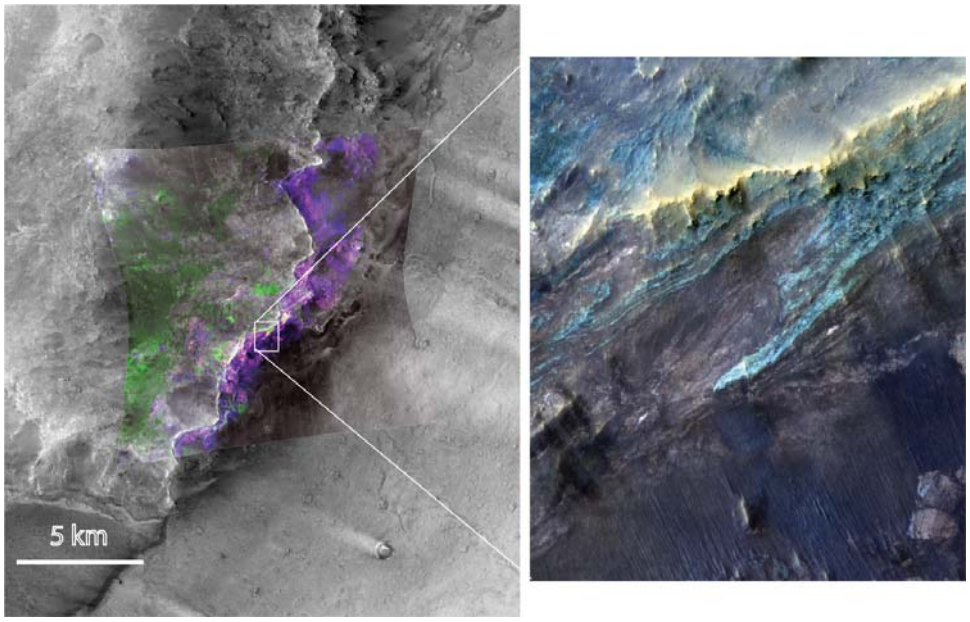

Figure 15. (left) Parameter map (R, BD1900; G, LCPINDEX; B, D2300) from CRISM image FRT00009D44 overlain on a subset of CTX image P16_007200_2002 along the western wall of the southern portion of Nili Fossae trough. Low-Ca pyroxene appears green, and phyllosilicates are blue to magenta. (right) The enlarged image of the wallrock shows a subset from HiRISE infrared color image PSP_007200_2005. Low-Ca pyroxene appears green, and phyllosilicates are brown. LCP and Fe/Mg-smectite are interlayered with the LCP. Layered breccia blocks within the wallrock unit are shown in the lower right corner of the inset.

graphic relationships shown in Figures 7, 9, and 10 to be a clear indication of draping of the olivine unit over preexisting basement topography. In Figure 10 the apparent layers of the olivine-bearing units are basal in the crater floor and are tilted up around the central mound. The distinctive stratigraphy of the mafic cap paired with a basal unit showing a stronger olivine spectral signature that is draped over topography is thus observed over 2000 km in distance across 2.5 km in elevation.

[38] This region in southern Isidis was examined in detail by *Tornabene et al.* [2008] with THEMIS data and they noted the erosion of olivine and mafic cap from the center mound region as well as upturned layers around the central mound as shown by HiRISE data. They argued that this was volcanic fill in Hashir crater associated with their hypothesis of regional olivine-rich volcanism. However, the mafic units in Hashir do not fill the crater interior to the rim nor is the rim breached. In addition, there are no volcanic rocks evident embaying the crater exterior walls to a level that might indicate it reached to the rim and spilled into the crater to fill the floor. If this were volcanic fill, there would need to be a vent strategically placed in the crater to emplace volcanic rocks in the crater.

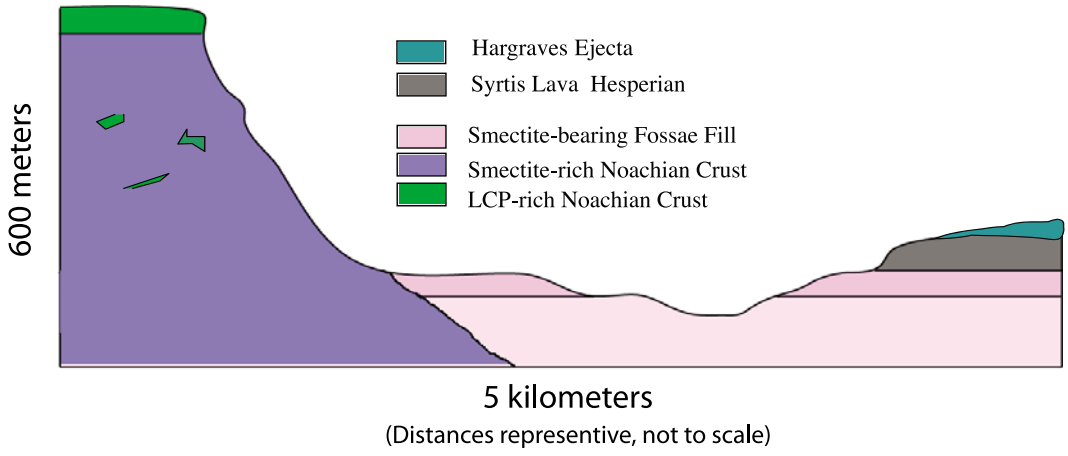

Figure 16. Representative cross section from the western edge of Figure 11 to the middle of the scene where ejecta from the Hargraves crater are observed.

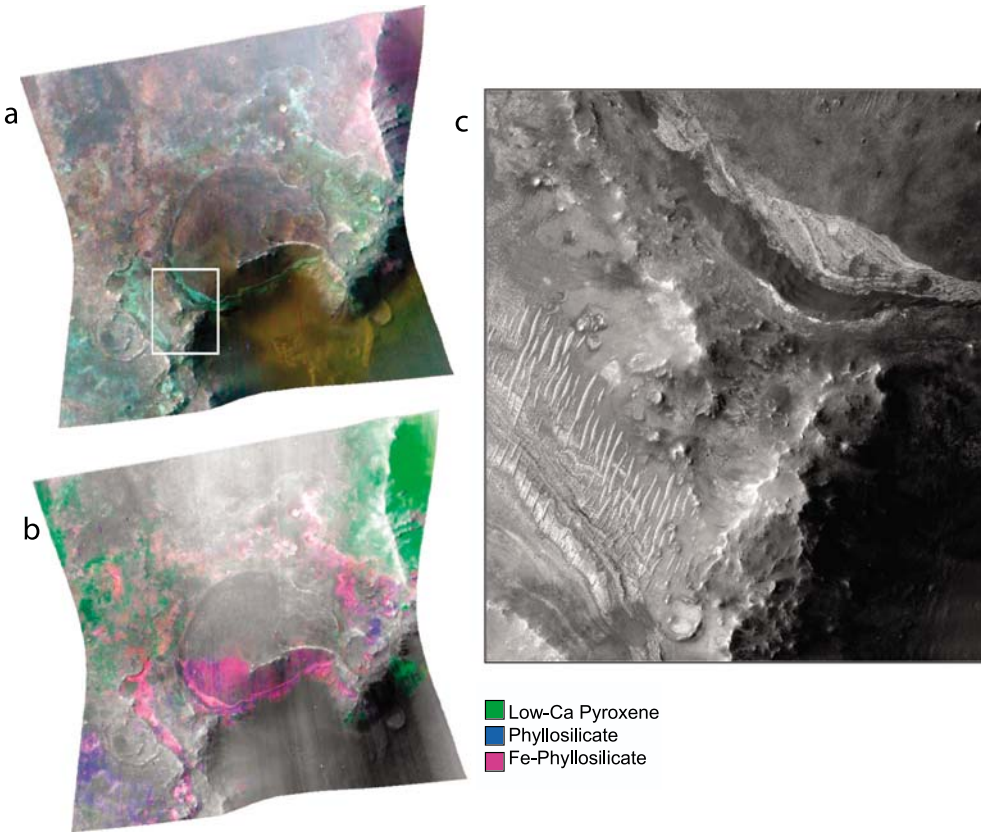

Figure 17. (a) False color CRISM image FRT0000BEC0 (R, 2.42; G, 1.81; B, 1.08 μm) taken of a filled crater cut by the fossae located just north of Figure 15. (b) Parameter map (R, BD1900; G, LCPINDEX; B, D2300) of Figure 17a in which low-Ca pyroxene appears green and phyllosilicates are blue to magenta. (c) Subset of HiRISE image PSP_009494_2010_RED showing layers within the Fe/Mg-smectite-bearing sedimentary fill, cropping out from beneath a mineralogically unremarkable mantling unit.

[39] A number of hypotheses have been proposed to explain the occurrence of olivine in this region. *Hoefen et al.* [2003] suggested the presence of an olivine-rich layer in the curst prior to Isidis that was exposed by the basing-forming event while *Hamilton and Christensen* [2005] proposed that mafic volcanic flows emplaced on the surface also prior to the Isidis event best explain the observations. Neither hypothesis seems likely given the location with the transient cavity of the Isidis basin and the unit's stratigraphic and superposition relationships. *Tornabene et al.* [2008] analyzed compositional and stratigraphic relationships of the olivine-bearing unit along the southern edge of the Isidis basin with TES and THEMIS data. They clearly defined a mafic cap unit overlying an olivine-rich unit, and concluded the olivine-rich units are picritic lavas emplaced subsequent to the formation of the Isidis basin. They suggest the lavas were fed by widespread, diffuse volcanism that was facilitated by fractures and structural weaknesses associated with the Isidis impact. The rising plumes that ultimately coalesced to form the Syrtis Major volcanic center exploited these zones of weaknesses.

[40] However, there are aspects of the observations that are not well accommodated by the volcanic hypothesis. This widespread volcanism traverses over 2.5 km of exposed elevation and yet did not leave distinct vents, fissures, edifices and constructs. They may have been removed by erosion or buried by later volcanism but the topographic and geographic extent of the distinctive mafic cap and olivine-rich strata requires a widespread diffuse volcanic emplacement processes of consistent composition. The olivine-mafic cap deposits are also observed lining the floor of an impact crater (Hasher, Figure 9c), with no clear source regions or process to emplace the unit as lava.

[41] Drawing from the example of the Orientale basin, *Mustard et al.* [2007] concluded that the timing, topographic range, and morphologic expression was most consistent with the emplacement and solidification of an impact melt sheet. The new data and our analyses lend some support to that hypothesis. The impact melt sheet hypothesis explains the broad topographic and geographic range of the olivine unit as seen now at submeter-scale resolution. The olivine unit with the associated mafic cap is found where the bedrock geology is well exposed in the northwest and southwest region of Isidis basin, the area proposed to be between the inner and outer rings [*Schultz and Frey*, 1990]. Across this large region it displays the same morphological and stratigraphic characteristics. The olivine deposits are clearly cut by the fossae in the region and do not show any evidence for flowing over the scarp walls or filling the fossae floor. Nili Fossae is veneered by lava from Syrtis Major, but this is distinct from the olivine-mafic cap unit. The fact that olivine deposits are cut by the fossae presents a specific time window for the emplacement

of the olivine unit. The unit is emplaced after the Isidis impact event but prior to the formation of the fossae. The fossae are poorly dated but *Wichman and Schultz* [1989] propose formation was shortly after the formation of the Isidis basin.

[42] A melt sheet emplaced as a consequence of the basin-forming event creates an effectively instantaneous deposit that is thus simultaneous with the basin formation but prior to the fossae formation. The emplacement of the olivine-rich unit by volcanism places this similarly very early after the formation of the Isidis basin, but the eruption process would need to have been completed by the time of the formation of the fossae.

[43] The distinct banding is a somewhat puzzling characteristic of the olivine unit. The thickness of individual bands and their apparent lateral continuity imply a sequential depositional process. Yet the layers conform to the contact with the basement units through depressions and over mounds (e.g., Figures 7 and 10). This draping character is difficult to accommodate through the emplacement of a low-viscosity fluid such as picritic volcanic flows that should fill topographic lows and any layering would be truncated against topographic change. The viscosity of a magmatic melt may be modified by the crystal content but ultramafic lavas are quite typically very low viscosity. Volcanic emplacement may have evolved as described but later deformed by tectonic processes resulting the observation of the olivine-mafic cap unit conforming to topography. However, except where cut by the fossae, we do not observe faulting in the olivine-mafic cap units that would be common in the case of widespread deformation.

[44] Conversely, an impact melt sheet with properties sufficient to drape topography (e.g., Maunder formation [*Head et al.*, 1993] would need to be somewhat viscous. The concentration of olivine at the base of the proposed melt sheet could be due to settling of olivine crystals precipitated from the melt or crystalline olivine fragments excavated from the mantle. But a melt with viscosity sufficient to drape or conform to topography might not be fluid enough to permit settling of olivine toward the base of the unit.

[45] There are several sources of apparent layering in impact melt. First, impact melt sheets undergo cooling and solidification subsequent to their emplacement and develop layer-like structures linked to cooling units, in a manner similar to thick, cooling basaltic lava flows. These structures are on the scale of meters to tens of meters. Second, interbedding is observed between crystalline melt units, suevite-like units, and more clast-rich breccia units [e.g., *Masaitis et al.*, 1999]. Third, layered units can develop due to differentiation of the melt sheet, as in the case of the Sudbury melt sheet [e.g., *Deutsch et al.*, 1995]. Together, these sources can produce a wide variety of layered and layer-like units as are often observed in terrestrial impact crater melt sheets.

[46] The olivine-mafic cap deposit is cut by the fractures that define the Nili Fossae (Figures 4 and 9c) as well as fluvial channels that traverse the Nili Fossae region [*Mangold et al.*, 2007]. For the most part the olivine-bearing unit is not altered. However, *Mangold et al.* [2007] noted a region of high thermal inertia that showed combined mafic and alteration signatures that they suggested was alteration of the olivine unit, and there are several distinct regions observed with MRO data associated with carbonate [*Ehlmann et al.*, 2008b] and serpentine [*Ehlmann et al.*, 2009a, 2009b]. There has been alteration of the mafic silicate units, and in places it is significant. But other regions clearly preserve unaltered units showing that there was a highly variable interaction of water with the rocks.

[47] The extensive fill of troughs and craters with phyllosilicate-bearing sediments points to a period of significant and widespread erosion, transport, and deposition. Analysis of topographic profiles across craters with and without fill shows the amount of fill in some places to be on the order of a kilometer [*Ehlmann et al.*, 2009a]. The amount of fill in the troughs is not determined at this time but sedimentary deposits beneath the Hesperian lavas are clearly seen on the trough floors. Sedimentary deposits associated with fluvial channels are also seen in the smaller fossae such as the area of Figure 4. Determining when this period of significant gradation occurred is difficult. The sedimentation in the Nili Fossae trough and other fossae was largely complete prior to the emplacement of the Early Hesperian Syrtis Major lava. Except for very minor, possible fan deposits [*Mangold et al.*, 2007] none of the sapping channels that exit to the Nili Fossae trough emplace sediment over the lava. The only significant deposit overlying the trough lavas is ejecta from Hargraves crater (Figures 11, 12, and 15).

[48] As shown in Figure 17, a crater cut by the trough displays finely layered sediment. The location of this crater near the putative rim of the Isidis basin indicates the fill is likely to have occurred after basin formation. The crater with the fill may have been present prior to the Isidis basin formation but it would have been covered by as much as a kilometer of ejecta that would need to have been removed to expose these finely layered sediments. The layers are exposed in this region by erosion along the western scarp of the Nili Fossae trough. This provides an upper limit on the timing of the fill that was likely completed by the time the trough formed. Thus, the period of gradation and sedimentary transport began prior to the opening of the fossae but continued after they had opened until the emplacement of the Hesperian Syrtis major lavas.

5. Conclusions

[49] The stratigraphic and superposition relationships among the major geologic units and events in this region can be ordered to provide a conceptual overview of major events that affected the area (Figure 18). As has been well document by numerous studies [e.g., *Bibring et al.*, 2005, 2006; *Poulet et al.*, 2005; *Mustard et al.*, 2008], widespread and pervasive formation of hydrated silicates, notably phyllosilicates, occurred during the Noachian era. In the Isidis-Nili Fossae region we can definitively date the deep crustal alteration to prior to the Isidis impact [*Mustard et al.*, 2007; *Mangold et al.*, 2007]. The crust that was impacted to form the basin contained extensive deposits of altered crust Some of the breccia blocks show characteristic subparallel layering implying that fluvial-lacustrine or eolian sedimentary systems existed prior to the basin formation. Some blocks show both unaltered and altered lithologies, perhaps preserving alteration fronts. The distinctive olivine-bearing unit found around the Nili Fossae and in Libya Montes was emplaced contemporaneous with or shortly after the formation of the

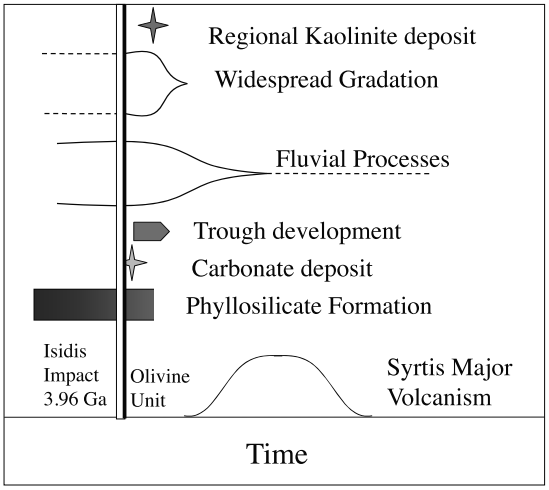

Figure 18. Schematic timeline of the geological history of the circum-Isidis region from the Noachian through the emplacement of the Syrtis Major volcanic rocks in the Hesperian.

Isidis basin and we interpret this to be impact melt. The olivine unit shows evidence for alteration [*Mangold et al.*, 2007; *Ehlmann et al.*, 2008b, 2009a, 2009b] but it is relatively minor. Because olivine is readily altered, this shows that the magnitude of alteration processes at the surface were minimal following the emplacement of the olivine unit. However, it is not known in what geologic environment pervasive Noachian alteration occurred (i.e., deep or shallow crust? Hydrothermal? Surface and pedogenic processes? A combination of processes?). Our analyses do show that surface or near-surface alteration processes were limited following the basin formation to formation of thin units of kaolinite and carbonate. There was nevertheless a significant period of gradation in which large volumes of rocks were eroded and transported to topographic lows, presumably by fluvial systems. While the magnitude of the gradation during this period was apparently large, filling craters with >1 km of sediment, only a few distinctive systems that preserve valley networks and depositional sites are observed. The most distinctive is the valley networks and delta deposits associated with the Jezero crater [*Fassett and Head*, 2005; *Ehlmann et al.*, 2008a] though there are other fluvial channels in the region, including evidence for surge channels or episodic outflow on the Syrtis Major volcanics [*Mangold et al.*, 2008].

[50] Regional hydrological activity had waned by the time of emplacement of the Syrtis Major lava flows, in agreement with the global model of progressively more water-limited conditions of alteration from the Hesperian onward proposed by *Bibring et al.* [2006]. However, the nature of the Noachian crust exposed in the circum-Isidis region points to the primacy of both geomorphological and geochemical processes driven by the action of liquid water in shaping early Mars and, in fact, to multiple iterations of these processes. Post-Isidis gradation was at least partially driven by fluvial activity. Furthermore, in the very earliest crust, the breccia blocks within the eroded basement unit at Nili Fossae have subparallel layers within smectite clay-rich rock. Hence, aqueous alteration and perhaps fluvial activity predate and were coincident with the period of large basin formation, indicating the early role of aqueous processes acting on Mars' original crust.

[51] **Acknowledgments.** The DEM from HiRISE image PSP_002176_2025 was produced by Ryan Ollerenshaw, Shigeru Suzuki, and Eric DeJong at the Jet Propulsion Laboratory Imaging Processing Laboratory. Support from NASA and the operation of the Mars Reconnaissance Orbiter is gratefully acknowledged. J.F.M. also acknowledges a contract from the Jet Propulsion Laboratory to participate on the OMEGA Team as a Liaison Member from the CRISM Team, and J.W.H. acknowledges support from a contract from the Jet Proposal Laboratory for participation in the Mars Express High-Resolution Stereo Camera (HRSC).

References

Arvidson, R. E., et al. (2006), Nature and origin of the hematite-bearing plains of Terra Meridiani based on analyses of orbital and Mars Exploration rover data sets, *J. Geophys. Res.*, *111*, E12S08, doi:10.1029/2006JE002728.

Bibring, J.-P., et al. (1989), Results from the ISM experiment, *Nature*, *341*, 591–592, doi:10.1038/341591a0.

Bibring, J.-P., et al. (2005), Mars surface diversity as reveal by the OMEGA/Mars Express observations, *Science*, *307*, 1576–1581, doi:10.1126/science.1108806.

Bibring, J.-P., et al. (2006), Global mineralogical and aqueous Mars history derived from OMEGA/Mars Express data, *Science*, *312*, 400–404, doi:10.1126/science.1122659.

Delamere, W. A., et al. (2009), Color imaging of Mars by the High Resolution Imaging Science Experiment (HiRISE), *Icarus*, doi:10.1016/j.icarus.2009.03.012, in press.

Deutsch, A., et al. (1995), The Sudbury structure (Ontario, Canada): A tectonically deformed multi-ring impact basin, *Geol. Rundsch.*, *84*, 697–709, doi:10.1007/s005310050034.

Ehlmann, B. L., J. F. Mustard, C. I. Fassett, S. C. Schon, J. W. Head III, D. J. DesMarais, J. A. Grant, and S. L. Murchie (2008a), Clay-bearing minerals and organic preservation potential in sediments from a Martian delta environment, Jezero crater, Nili Fossae, Mars, *Nat. Geosci.*, *1*, 355–358, doi:10.1038/ngeo207.

Ehlmann, B. L., et al. (2008b), Orbital identification of carbonate-bearing rocks on Mars, *Science*, *322*, 1828–1832, doi:10.1126/science.1164759.

Ehlmann, B. L., et al. (2009a), Identification of hydrated silicate minerals on Mars using MRO-CRISM: Geologic context near Nili Fossae and implications for aqueous alteration, *J. Geophys. Res.*, *114*, E00D08, doi:10.1029/2009JE003339.

Ehlmann, B. L., J. F. Mustard, and S. L. Murchie (2009b), Detection of serpentine on Mars by MRO-CRISM and possible relationship with olivine and magnesium carbonate in Nili Fossae, *Lunar Planet. Sci.*, *XL*, Abstract 1787.

Fassett, C. I., and J. W. Head III (2005), Fluvial sedimentary deposits on Mars: Ancient deltas in a crater lake in the Nili Fossae region, *Geophys. Res. Lett.*, *32*, L14201, doi:10.1029/2005GL023456.

Hamilton, V. E., and P. R. Christensen (2005), Evidence for extensive, olivine-rich bedrock on Mars, *Geology*, *33*, 433–436, doi:10.1130/G21258.1.

Head, J. W., and J. F. Mustard (2006), Breccia dikes in impact craters on Mars: Erosion and exposure on the floor of a 75-km diameter crater at the dichotomy boundary, *Meteorit. Planet. Sci.*, *41*, 1675–1690.

Head, J. W., S. Murchie, J. F. Mustard, C. M. Pieters, G. Neukum, A. McEwen, R. Greeley, E. Nagel, and M. J. S. Belton (1993), Lunar impact basins: New data for the western limb and far side (Orientale and South Pole-Aitken basins) from the first Galileo flyby, *J. Geophys. Res.*, *98*, 17,149–17,181, doi:10.1029/93JE01278.

Hiesinger, H., and J. W. Head (2004), The Syrtis Major volcanic province, Mars: Synthesis from Mars Global Surveyor data, *J. Geophys. Res.*, *109*, E01004, doi:10.1029/2003JE002143.

Hoefen, T. M., R. N. Clark, J. L. Bandfield, M. D. Smith, J. C. Pearl, and P. R. Christensen (2003), Discovery of olivine in the Nili Fossae region of Mars, *Science*, *302*, 627–630, doi:10.1126/science.1089647.

Malin, M. C., et al. (2007), Context Camera Investigation on board the Mars Reconnaissance Orbiter, *J. Geophys. Res.*, *112*, E05S04, doi:10.1029/2006JE002808.

Mangold, N., et al. (2007), Mineralogy of the Nili Fossae region with OMEGA/Mars Express data: 2. Aqueous alteration of the crust, *J. Geophys. Res.*, *112*, E08S04, doi:10.1029/2006JE002835.

Mangold, N., V. Ansan, D. Baratoux, F. Costard, L. Dupeyrat, H. Hiesinger, P. Masson, G. Neukum, and P. Pinet (2008), Identification of a new outflow channel on Mars in Syrtis Major Planum using HRSC/MEx data, *Planet. Space Sci.*, *56*(7), 1030–1042, doi:10.1016/j.pss.2008.01.011.

Masaitis, V. L., M. V. Naumov, and M. S. Mashchak (1999), Anatomy of the Popigai impact crater, Russia, in *Large Meteorite Impacts and Planetary Evolution II*, edited by B. O. Dressler and V. L. Sharpton, *Spec. Pap. Geol. Soc. Am.*, *339*, 1–17.

McEwen, A. S., et al. (2007), Mars Reconnaissance Orbiter's High Resolution Imaging Science Experiment (HiRISE), *J. Geophys. Res.*, *112*, E05S02, doi:10.1029/2005JE002605.

McEwen, A. S., L. Tornabene, J. Grant, J. Wray, and J. Mustard (2008), Noachian Megabreccia on Mars, *Eos Trans. AGU*, *89*(53), Fall Meet. Suppl., Abstract P43D-03.

McGuire, P. C., et al. (2009), An improvement to the volcano-scan algorithm for atmospheric correction of CRISM and OMEGA spectral data, *Planet. Space Sci.*, *57*, 809–815, doi:10.1016/j.pss.2009.03.007.

Michalski, J. R., F. Poulet, J.-P. Bibring, and N. Mangold (2009), Combined visible/near infrared and thermal infrared analyses of the Nili Fossae region, Mars, *Lunar Planet. Sci.*, *XL*, Abstract 1365.

Murchie, S., et al. (2007a), Compact Reconnaissance Imaging Spectrometer for Mars (CRISM) on Mars Reconnaissance Orbiter (MRO), *J. Geophys. Res.*, *112*, E05S03, doi:10.1029/2006JE002682.

Murchie, S., E. Guinness, and S. Slavney (2007b), CRISM Data Product Software Interface Specification, ftp://pds-geosciences.wustl.edu/crism-edr01/mro-m-crism-2-edr-v1/mrocr_0001/document/crism_dpsis.pdf, Planet. Data Syst., Greenbelt, Md., 17Aug.

Mustard, J. F., F. Poulet, A. Gendrin, N. Mangold, J.-P. Bibring, Y. Langevin, B. Gondet, G. Bellucci, F. Altieri, and the OMEGA Science Team (2005), Olivine and pyroxene diversity in the crust of Mars, *Science*, *307*, 1594–1597, doi:10.1126/science.1109098.

Mustard, J. F., F. Poulet, J. W. Head, N. Mangold, J.-P. Bibring, S. M. Pelkey, C. I. Fassett, Y. Langevin, and G. Neukum (2007), Mineralogy of the Nili Fossae region with OMEGA/Mars Express data: 1. Ancient impact melt in the Isidis basin and implications for the transition from the Noachian to Hesperian, *J. Geophys. Res.*, *112*, E08S03, doi:10.1029/2006JE002834.

Mustard, J., et al. (2008), Hydrated silicate minerals on mars observed by the CRISM instrument on MRO, *Nature*, *454*, 305–309, doi:10.1038/nature07097.

Pelkey, S. M., et al. (2007), CRISM multispectral summary products: Parameterizing mineral diversity on Mars from reflectance, *J. Geophys. Res.*, *112*, E08S14, doi:10.1029/2006JE002831.

Poulet, F., J.-P. Bibring, J. F. Mustard, A. Gendrin, N. Mangold, Y. Langevin, R. E. Arvidson, B. Gondet, and G. Gomez (2005), Phyllosilicates on Mars and implications for the early Mars history, *Nature*, *438*, 623–627, doi:10.1038/nature04274.

Poulet, F., C. Gomez, J.-P. Bibring, Y. Langevin, B. Gondet, P. Pinet, G. Belluci, and J. Mustard (2007), Martian surface mineralogy from Observatoire pour la Minéralogie, l'Eau, les Glaces et l'Activité on board the Mars Express spacecraft (OMEGA/MEx): Global mineral maps, *J. Geophys. Res.*, *112*, E08S02, doi:10.1029/2006JE002840.

Salvatore, M. R., J. F. Mustard, M. B. Wyatt, S. L. Murchie, and O. S. Barnouin-Jha (2009), Assessing the mineralogy of Acidalia Planitia, Mars, using near-infrared orbital spectroscopy, *Lunar Planet. Sci.*, *XL*, Abstract 2050.

Schultz, R. A., and H. V. Frey (1990), A new survey of multiring impact basins on Mars, *J. Geophys. Res.*, *95*, 14,175–14,189, doi:10.1029/JB095iB09p14175.

Skok, J. R., J. F. Mustard, S. L. Murchie, and M. B. Wyatt (2009), Spectrally distinct ejecta in Syrtis Major, Mars: Evidence for environmental change at the Hesperian-Amazonian boundary, *J. Geophys. Res.*, doi:10.1029/2009JE003338, in press.

Stamnes, K., S.-C. Tsay, K. Jayaweera, and W. Wiscombe (1988), Numerically stable algorithm for discrete-ordinate-method radiative transfer in multiple scattering and emitting layered media, *Appl. Opt.*, *27*, 2502–2509, doi:10.1364/AO.27.002502.

Tanaka, K. L., J. S. Kargel, D. J. MacKinnon, T. M. Hare, and N. Hoffman (2002), Catastrophic erosion of Hellas basin rim on Mars induced by magmatic intrusion into volatile-rich rocks, *Geophys. Res. Lett.*, *29*(8), 1195, doi:10.1029/2001GL013885.

Taylor, G. J., et al. (2006), Bulk composition and early differentiation of Mars, *J. Geophys. Res.*, *111*, E03S10, doi:10.1029/2005JE002645.

Taylor, G. J., S. M. McLennan, H. Y. McSween Jr., M. B. Wyatt, and R. C. F. Lentz (2008), Implications of observed primary lithologies, in *The Martian Surface: Composition, Mineralogy and Physical Properties*, edited by J. F. Bell, pp. 508–518, Cambridge Univ. Press, New York.

Tornabene, L. L., J. E. Moersch, H. Y. McSween Jr., V. E. Hamilton, J. L. Piatek, and P. R. Christensen (2008), Surface and crater-exposed lithologic units of the Isidis basin as mapped by coanalysis of THEMIS and TES derived data products, *J. Geophys. Res.*, *113*, E10001, doi:10.1029/2007JE002988.

Werner, S. C. (2005), Major aspects of the chrono-stratigraphy and geologic evolutionary history of Mars, Ph.D. dissertation, Cuvilier, Berlin.

Wichman, R. W., and P. H. Schultz (1989), Sequence and mechanisms of deformation around the Hellas and Isidis impact basins on Mars, *J. Geophys. Res.*, *94*, 17,333–17,357, doi:10.1029/JB094iB12p17333.

J.-P. Bibring and F. Poulet, Institut d'Astrophysique Spatiale, Université Paris Sud, CNRS, F-91405 Orsay, France.

B. L. Ehlmann, J. W. Head, J. F. Mustard, and L. H. Roach, Department of Geological Sciences, Brown University, Box 1846, Providence, RI 02912, USA. (John_Mustard@brown.edu)

N. Mangold, Laboratoire de Planétologie et Géodynamique, Université de Nantes, CNRS, F-44000 Nantes, France.

S. L. Murchie, Johns Hopkins University Applied Physics Laboratory, Laurel, MD 20723, USA.